



Full length article

Tough and deformable glasses with bioinspired cross-ply architectures

Zhen Yin, Ahmad Dastjerdi, Francois Barthelat*



Department of Mechanical Engineering, McGill University, 817 Sherbrooke Street West, Montreal, QC H3A 2K6, Canada

ARTICLE INFO

Article history:

Received 2 February 2018

Received in revised form 3 May 2018

Accepted 9 May 2018

Available online 1 June 2018

Keywords:

Architected materials

Cross-ply

Glass

Three-dimensional laser engraving

Toughness

ABSTRACT

Glasses are optically transparent, hard materials that have been in sustained demand and usage in architectural windows, optical devices, electronics and solar panels. Despite their outstanding optical qualities and durability, their brittleness and low resistance to impact still limits wider applications. Here we present new laminated glass designs that contain toughening cross-ply architectures inspired from fish scales and arthropod cuticles. This seemingly minor enrichment completely transforms the way laminated glass deforms and fractures, and it turns a traditionally brittle material into a stretchy and tough material with little impact on surface hardness and optical quality. Large ply rotation propagates over large volumes, and localization is delayed in tension, even if a strain softening interlayer is used, in a remarkable mechanism which is generated by the kinematics of the plies and geometrical hardening. Compared to traditional laminated glass which degrades significantly in performance when damaged, our cross-ply architecture glass is damage-tolerant and 50 times tougher in energy terms.

Statement of Significance

Despite the outstanding optical qualities and durability of glass, its brittleness and low resistance to impact still limits its wider application. Here we present new laminated glass designs that contain toughening cross-ply architectures inspired from fish scales and arthropod cuticles. Enriching laminated designs with crossplies completely transforms the material deforms and fractures, and turns a traditionally brittle material into a stretchy and tough material – with little impact on surface hardness and optical quality. Large ply rotation propagates over large volumes and localization is delayed in tension because of a remarkable and unexpected geometrical hardening effect. Compared to traditional laminated glass which degrades significantly in performance when damaged, our cross-ply architecture glass is damage-tolerant and it is 50 times tougher in energy terms. Our glass-based, transparent material is highly innovative and it is the first of its kind. We believe it will have impact in broad range of applications in construction, coatings, chemical engineering, electronics, photovoltaics.

Crown Copyright © 2018 Published by Elsevier Ltd on behalf of Acta Materialia Inc. All rights reserved.

1. Introduction

With fast developments in the applications of glass in electronic devices, solar panels and windows for building and vehicles, there are increasing needs for tough and damage tolerant glass materials [1]. Toughness, which indicates the capability of a material to resist crack propagation and impacts, requires high strength and high deformability. However, strength and deformability are usually mutually exclusive in many traditional engineering materials [2]. Glass is a widely used material because of its hardness, optical properties, thermal and chemical stability, and durability. However, its range of applications is currently severely limited by its

low fracture toughness (Fig. 1a). Currently, the main two methods used to improve the mechanical performance of glass are tempering and lamination [3]. Tempering consists of generating residual compressive stresses at the surface of glass components by either heat treatment or ion implantation, in order to offset tensile stresses arising from external loading. However, once a crack is initiated in tempered glass, the release of elastic energy produces catastrophic and “explosive” failures which destroy the entire component into small fragments. Laminating glass is another strategy which consists of intercalating glass layers with softer polymeric layers to keep glass fragments together in case of fracture. However, the impact resistance of laminated glass is not significantly higher than plain glass because the deformability and toughness of the polymer layers are not fully exploited [3]. Recent work has suggested new pathways to transform the mechanics and improve

* Corresponding author.

E-mail address: francois.barthelat@mcgill.ca (F. Barthelat).

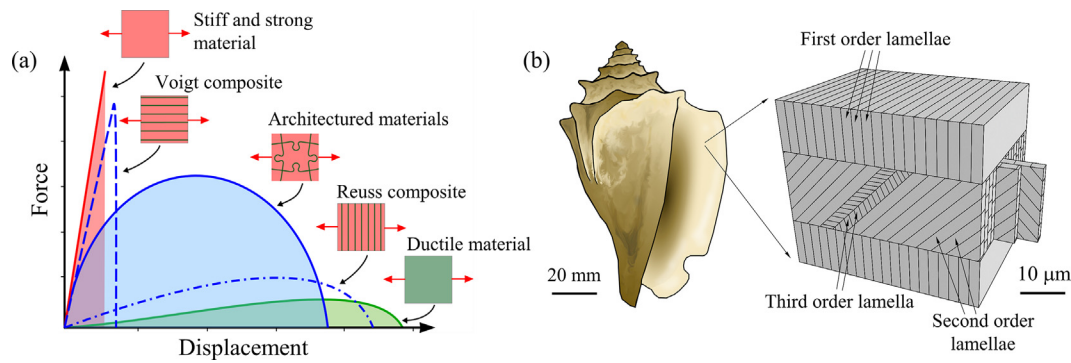


Fig. 1. (a) Generic force displacement curve for a stiff and strong (but brittle) material, a low-strength ductile material, and for three possible composites of these materials; (b) Cross-ply architectures in conch shell.

the properties of materials, by creating highly controlled material “architectures” at length scales intermediate between the micro-scale and the scale of the component.

This approach provides a promising way to exploit the synergies between constituents in a composite material and to achieve new combinations of properties [4]. Since morphological control is high, the shape, size and arrangement of the building blocks can be tailored to maximize overall material properties and generate new and useful combinations of strength and deformability (Fig. 1a). Interestingly, nature is well ahead of engineers in making use of architected materials [4]. Materials such as bone, teeth or mollusk shells are also made of stiff building blocks of well-defined sizes and shapes, bonded by deformable organic interfaces. The interplay between the building blocks and the non-linear behaviors at the interfaces generate powerful combinations of stiffness, strength and toughness not yet found in synthetic materials [4,5]. For example, Fig. 1b shows the architecture of conch shells, a remarkable material made of >95% vol. of brittle biominerals with a toughness three orders of magnitude higher than that mineral [6]. The architecture of conch shell consists of a series of cross-ply lamellae at different length scales [7,8], where mineral lamellae are separated and adhered by thin organic interfaces. Propagating cracks are deflected and guided by the weaker organic interfaces, which triggers powerful toughening mechanisms such as crack bridging [9,10]. Cross-ply architecture with similar toughening mechanisms can also be observed in the decussation zone of enamel [11]. The organic content in enamel only represents 1–5 wt% content but it contributes substantially to overall toughness [12]. Removing the protein interfaces in enamel can reduce the toughness by 40% [13]. Cross-ply architectures are also found in fish scales [14,15] and arthropod cuticles [16], generating powerful crack resisting mechanisms such as crack deflection, crack twisting, crack bridging, and process zone toughening [14,15,17]. In addition, the interfaces between the fibers in these materials can undergo large deformations [12], so that fibers can rotate and align with the pulling direction, strengthening the material along that direction. While nature presents spectacular examples of cross-ply architectures, attempts to systematically incorporate these bio-inspired designs in synthetic materials have been so far limited [18–20]. Here we combine the concepts of lamination in glass [3], highly controlled material architecture [4], laser-induced weak interfaces [21], highly deformable interlayers [12], and bioinspiration [9,11,22] to generate new types of glass with a superior combination of toughness, deformability and damage tolerance. We examine the effect of the architecture on micromechanics of deformation, overall performance, and fracture mechanics by using combinations of experiments and models.

2. Fabrication protocol

In this study, we used 0.22 mm thick standard borosilicate glass (Fisher Scientific, PA, USA) as the base material, combined with a continuous, 0.15 mm thick adhesive layer. A critical requirement for the adhesive is to be highly deformable at moderate stress in order to promote interlayer shearing over the fracture of the glass layers. To explore possible adhesives, we conducted single lap shear tests on a selection of adhesives using 1 mm thick borosilicate glass substrates. The adhesives were an ethylene-vinyl acetate (EVA, Caida, Tianjin, China), an ionomer (DuPont Surlyn, DE, USA), a cyanoacrylate (Adhesive System, IL, USA) and an epoxy (BMB Solutions Composites, QC, Canada). Force and displacement were converted to shear stress and shear strain using the surface area and thickness of the adhesive layer (Fig. 2). As expected, Cyanoacrylate and epoxy have high shear strength but very low deformability, making them unsuitable for our material. Surlyn show a combination of high shear strength (>10 MPa) and high shear strain at failure (>300%). However, preliminary experiments on the thinner glass slides used in our architected laminated glass showed extensive damage in glass because Surlyn is too strong. EVA was the most suitable for our material: it is optically transparent, it has strong adhesion on glass, and can undergo large inelastic deformations with energy dissipation. The shear strength of EVA is sufficiently low to promote yielding at the interlayer over brittle fracture of the glass substrates. Fig. 3 shows the fabrication protocol. A pair of plain glass plates was first covered with a heat resistant polyimide (PI) tape (McMaster-carr, IL, USA) to facilitate

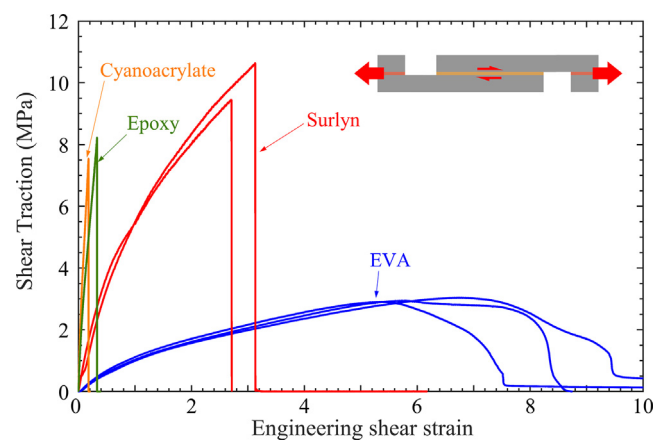


Fig. 2. The shear stress-strain curves from the single lap shear tests on EVA, Surlyn, cyanoacrylate and epoxy. The glass substrates failed in the tests of cyanoacrylate, epoxy and Surlyn.

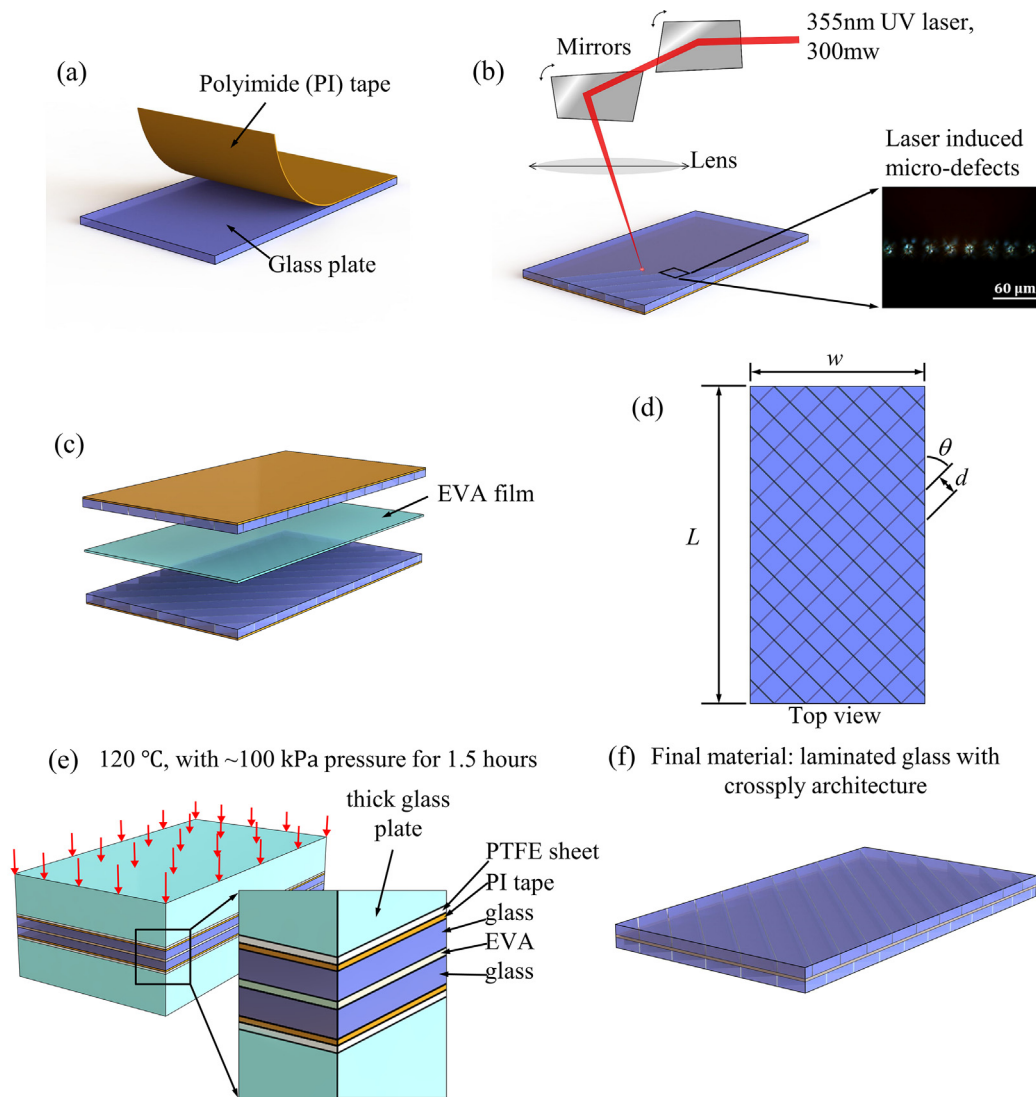


Fig. 3. Fabrication steps for the laminated cross-ply samples: (a) A polyimide film is attached to the glass plate; (b) laser engraving of weak interfaces into glass plates to form plies; (c) assembly of the laminated sample with $\pm\theta$ engraved plates; (d) top view showing the structure of the engraved lines with spacing d and angle $\pm\theta$ (e) Application of pressure and heat to soften EVA and create adhesion; (f) Final material: plate of architected cross-ply laminated glass.

the handling of the glass plate after laser engraving. Straight lines were then carved into the glass plates using a laser engraver (Vitro Laser solutions UG, Minden, Germany). These weak interfaces consisted of arrays of microcracks with 10 μm spacing, generated with the focused pulsed UV laser beam (355 nm, 300 mw). These microcracks were engraved through the entire thickness of the plates, following a pattern of parallel lines spaced by a distance d and at an angle θ from the long axis of the glass plates (Fig. 3b). The individual plies were then mechanically separated along the laser engraved lines, the PI tape holding the plate together for easier handling. A pair of these engraved plates was then assembled with a $\pm\theta$ orientation with the EVA film as interlayer to form a cross-ply architecture (Fig. 3c, d). This assembly was pressed with a uniform pressure of 100 kPa and kept at 120 $^{\circ}\text{C}$ in an oven for 1.5 h in order for the EVA layer to develop a strong adhesion to the glass plates (Fig. 3e). The assembly was then slowly cooled to room temperature, which produced the final material (Fig. 3f). In this study, we explored different architectures with ply angles of $\theta = \pm 45^{\circ}$, $\pm 60^{\circ}$ and $\pm 75^{\circ}$ for tensile tests and an additional $\theta = \pm 15^{\circ}$ for the fracture tests. The ply width was varied from $d = 1$ mm, 2 mm and 3 mm for both tensile and fracture tests. These ply angles and ply widths

were chosen because they lead to the wide range of failure modes described below. The process of laser engraving may leave some roughness on the cut surfaces, but the glass faces were not affected and the interfaces between the glass faces and the interlayer remained intact and smooth. For reference, we also prepared traditional, “plain” laminated glass plates which were assembled using the same protocol shown on Fig. 3, but where the laser engraving step was skipped. Plain and architected laminated plates were then cut into their final shapes: dogbone specimens for tensile tests, and compact tension specimens for fracture tests.

3. Optical quality

A natural concern for laser engraving features in glasses is their impact on optical quality. Fig. 4a shows the results of the light transmittance [23,24] at different light wavelengths for plain laminated glasses and for cross-ply architected glasses. Even with a relatively dense ply formation ($d = 1$ mm, $d/w = 0.1$), the cross-ply architected glasses show excellent transmittance in the visible light spectrum (wavelength 380–780 nm). We also assessed opti-

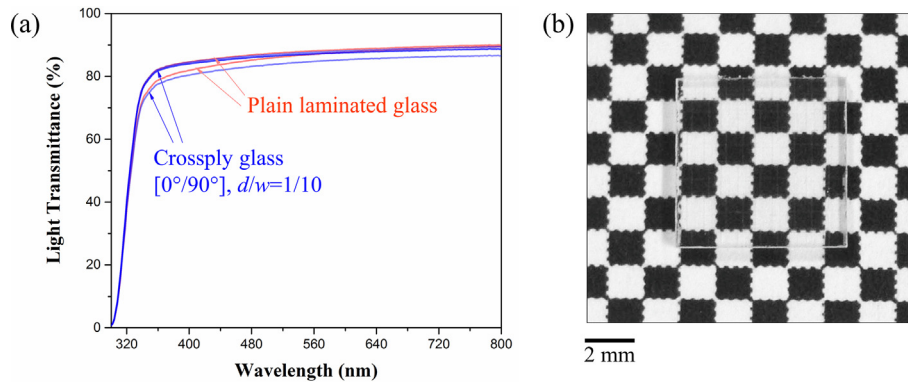


Fig. 4. Optical properties of the plain and architected laminated glasses: (a) light transmittance and (b) optical clarity: No decrease in light transmittance, image distortion or decrease in the appearance of objects was observed for the architected materials.

cal clarity, which is the property of transmitting light without spatial distortions [25]. Fig. 4b shows our materials in front of a checkered background, showing little effect on contrast and resolution, and no distortion of the pattern viewed through the materials. The impact of laser engraving on the optical quality of the laminated glass panels was therefore not significant.

4. Tensile tests

Tension is the loading configuration where glasses and traditional laminated glasses perform the poorest in term of strength, brittleness and energy absorption. Tensile tests were therefore well suited to highlight how our augmented cross-ply designs can address brittleness in traditional glass materials. For these tests, we prepared dogbone-shaped laminated samples with the dimensions shown on Fig. 5a (adapted from ASTM C1273 [26]). Nine combinations of ply width d and ply angle θ were explored, and 3–5 samples were tested for each combination. The pictures shown in Fig. 5 (and other similar pictures in this paper) were captured with a C-5060 Olympus digital camera using a black background and a bright illumination from an angle that highlighted the engraving lines. In normal conditions of illumination, these lines

were barely visible (see optical tests above). The samples were mounted on a miniature loading stage (E. Fullam, NY) and stretched at a constant rate of 10 $\mu\text{m/s}$. The samples were considered to have failed once the glass architecture had completely collapsed, at which point only the EVA interlayer provided a small tensile force.

The characteristic length scale for our architecture (ply width $d = 1, 2$ or 3 mm) is relatively close to the size of the sample (fixed sample width $w = 6$ mm, Fig. 5a), so that the usual separation of length scales between microstructure and component size cannot be applied [27]. An important implication is that homogenization of properties is not valid, and that the usual concepts of stress and strains had to be used with caution. For this reason, we used the normalized displacement u/L to characterize deformations, where u is the applied displacement and L is the effective length of the tensile test specimens ($L = 12$ mm for all samples, Fig. 5a). We also used an “apparent” nominal stress F/A to characterize internal tractions in the material, where F is the tensile force on the material and A is the cross-sectional area ($A = 3.6$ mm² for all samples). Fig. 5b shows typical tensile responses for pure EVA film, traditional laminated glass, and a cross-ply architected glass. Pure EVA displayed a relatively low tensile strength (~ 2 MPa), but very large extensions (strain at failure $>700\%$). In contrast,

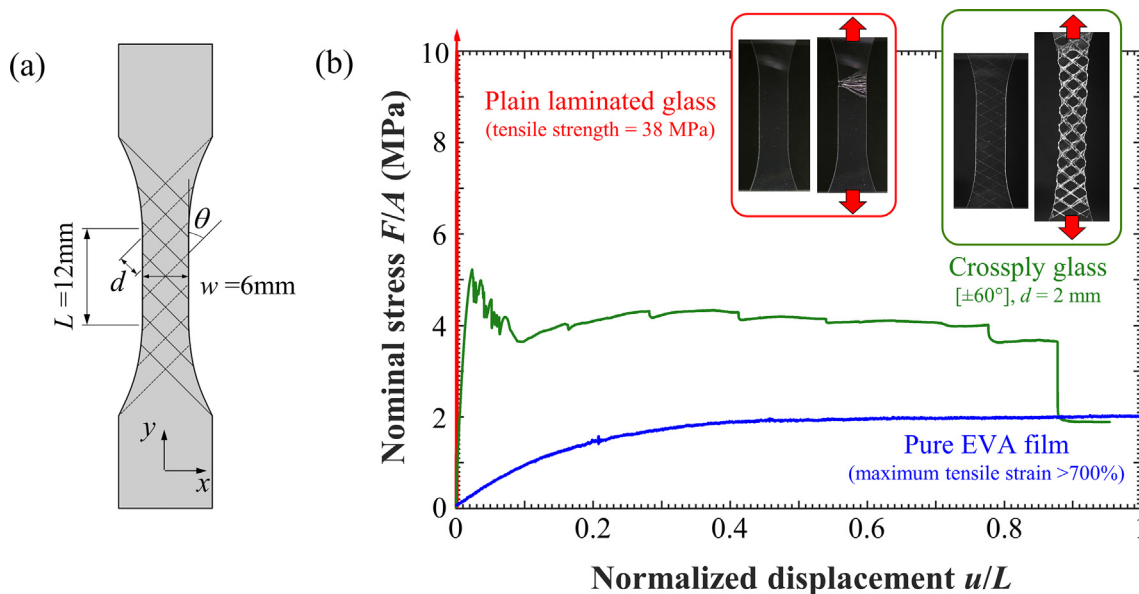


Fig. 5. (a) Overview of tensile test samples; (b) typical tensile responses for pure EVA, traditional laminated glass and cross-ply architected glass.

the laminated glass was very stiff and strong (strength = 38 MPa) but brittle (strain at failure <0.3%) with multiple catastrophic cracks localized in a small region (Fig. 5b). This strong but brittle behavior is typical for laminated glasses. The configuration of the laminated glass in tension corresponds to a “uniform strain” composite, where the glass layers carry most of the tensile force because they are much stiffer than the EVA interlayer. While the deformable interlayer can hold glass debris together in case of fracture, it generates little improvements in strength, energy absorption or impact resistance [3]. The polymeric interlayer in traditional laminated glasses has a large capacity of absorbing impact energy, but only a small and localized volume fraction of that interlayer is deformed in case of impact and fracture (Fig. 5b). The architected cross-ply glass produced a tensile response which was intermediate between the laminated glass and pure EVA (Fig. 5b). Compared to traditional laminated glasses, the architected glasses have a lower strength, but they are several orders of magnitude more ductile which translated into much larger energy absorption. They also fail progressively and in a more “graceful” fashion, which contrasts with laminated glass. These large deformations are generated by the separation, sliding and rotation of the plies over large volumes, which involves large shearing deformations in the EVA interlayer (Fig. 5b and Fig. 6). Ply delamination, sliding, and rotation are common mechanisms in collagen cross-ply in fish scales [14,15] and chitin Bouligand plies in arthropod cuticles [28,29]. Fig. 6 shows the tensile response for cross-ply architected glasses with $\theta = \pm 45^\circ$, $\pm 60^\circ$ and $\pm 75^\circ$ and with $d = 2$ mm, together with snapshots of the samples taken during the tensile tests. We observed several distinct failure modes depending on ply width and ply angle. Low ply angles ($\theta = \pm 45^\circ$) lead to the high strength, but some plies failed prematurely, leading to premature strain localization and failure. In these cases, most of the plies did not separate, and most of the interlayer deformed within small strains. The material with a ply

angle of $\theta = \pm 60^\circ$ led to a slightly lower strength, but much greater deformations. In these materials, every ply separated and rotated by as much as $10\text{--}12^\circ$ towards the direction of pulling. This “rotational mode” was prominent in $\theta = \pm 60^\circ$ samples. This mechanism involves the shear deformation of large volumes of the EVA interfaces, which translates into very high overall deformation and energy absorption. The $\theta = \pm 60^\circ$ samples eventually failed by the brittle fracture of one or more plies, which occurred at tensile deformation of almost 100%. Samples with high ply angle ($\theta = \pm 75^\circ$) had a slightly lower tensile strength and also displayed early localization of deformations, which in turn led to relatively low deformation at failure and low energy absorption. The plies separated and slid on one another and their rotation was minimal. This “translational mode” appears to be prominent for high ply angles. Fig. 6 shows that the deformation and energy dissipation both increase when the volume of deformed material is larger. The results also show how the geometry of the plies can be tuned to achieved optimum strength (this effect is explored in detail in Section 5 below). We also assessed the effects of ply width d , by testing samples with $d = 1$ mm (corresponding to $d/w = 1/6$), $d = 2$ mm ($d/w = 1/3$) and $d = 3$ mm ($d/w = 1/2$) with ply angles of $\theta = \pm 45^\circ$, $\pm 60^\circ$ and $\pm 75^\circ$ for each width. Fig. 7 provides a summary and deformation map for the nine different geometries considered here. Remarkably, we found that the failure mode was primarily affected by the ply angle but not affected by ply width. For example, all samples with $\theta = \pm 75^\circ$ failed by translational mode, but the failure was much localized for $d = 3$ mm. The stiffness and the strength of the materials also increased when d was increased, because increasing d increases the overlap area between the plies, which in turn increases the forces required for ply separation and rotation.

The properties obtained for these various cross-ply geometries are summarized on Fig. 8. The stiffness of the cross-ply architected glasses ranges from 0.3 to 0.8 GPa, which is about 20 times lower than plain laminated glass (~ 15 GPa). However, the strength of the cross-ply architected glasses is also 100 times higher than plain EVA (~ 8 MPa), because the cross-ply architecture turns the deformation of the EVA from tension into shear, which grants larger force with the same cross-section area. The cross-ply architected glasses are about five times weaker than laminated glass in terms of static strength (p -value $p < 0.05$ from a one tailed unpaired sample t -test, Fig. 8b), but they can deform up to 400 times more and they can absorb about 100 times more mechanical energy (Fig. 8c and d). The progressive failure and large energy absorption of the cross-ply architected materials is the result of the delocalized deformation induced by the cross-ply architecture. The geometry of the cross-ply has a strong effect on mechanical response, with lower ply angles θ and higher ply width d favoring high stiffness and high strength. However, for energy dissipation, intermediate values ($\theta = 60^\circ$ and $d = 2$ mm) led to the best performance. The mechanical response of the architected laminated glass is the result of a competition between brittle ply fracture, translational ply sliding and ply rotation. As ply width is increased, the overlap between the plies increases and the force transmitted between plies across the interlayer increases. Small ply width ($d = 1$ mm) lead to small overlap, and in general to low strength and energy absorption. In contrast, wider plies ($d = 3$ mm) generate large overlaps and higher strength, but excessive stresses within the plies lead to ply fracture, which limits the amounts of energy absorbed. In this work plies of width $d = 2$ mm provided the best performance in terms of combined strength and energy absorption. This optimum between interface strength, ply strength and overlap is similar to the mechanics and optimization of brick-and-mortar composites [30]. We explore how ply angle affect the results and lead to an optimum of $\theta = 60^\circ$ in the next section.

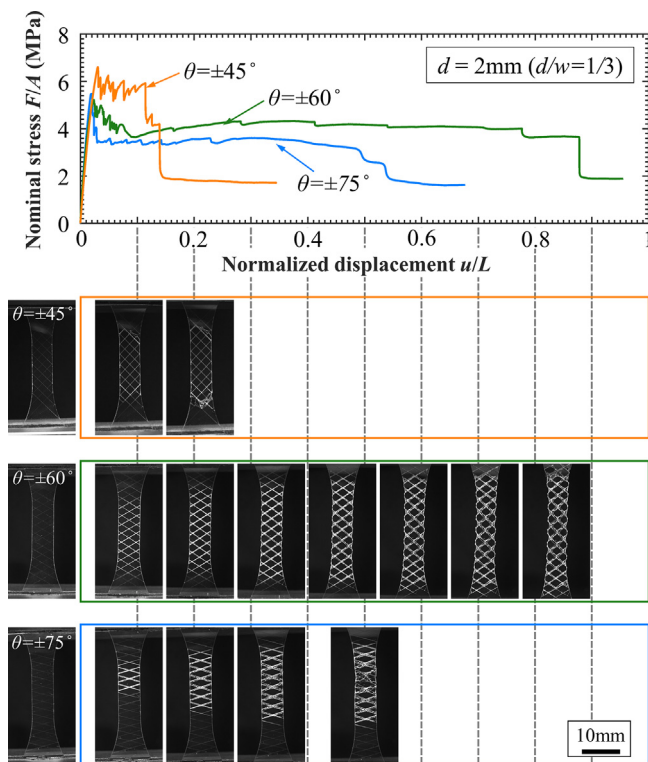


Fig. 6. Tensile response and associated deformation mechanisms for cross-ply-architected glasses with $\theta = 75^\circ$, 60° and 45° . For all configurations $d = 2$ mm (corresponding to $d/w = 1/3$).

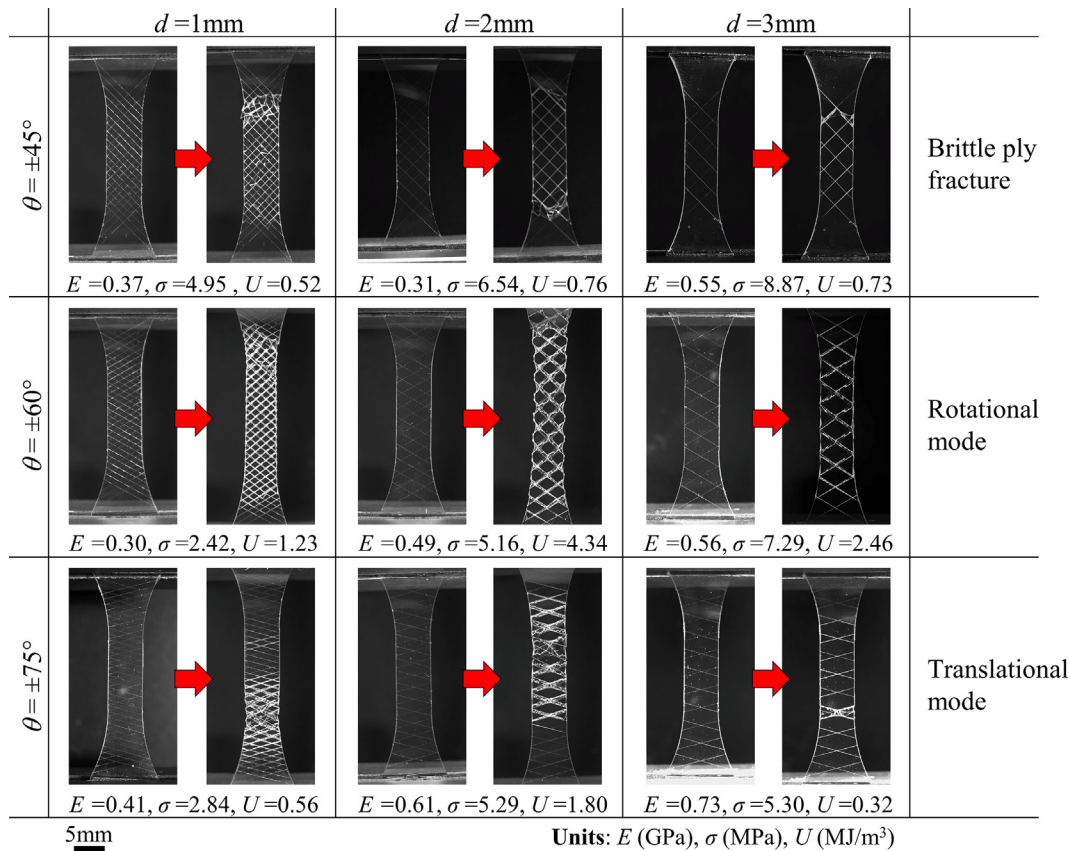


Fig. 7. Deformation map showing three tensile deformation and failure modes for cross-ply architected glasses as function of ply angle and ply width, supplied with stiffness E , strength σ , and unit volume energy absorption U for each configuration.

5. Finite elements model and analysis

For a better understanding of the mechanisms that govern the deformation and failure modes and the overall properties of the cross-ply, we modeled the cross-ply architected samples in tension using finite elements (ANSYS 16.0, PA, US [31]). Fig. 9a shows the 3D geometry and the loading conditions of the finite element model. The glass plies were modeled as linear isotropic elastic with an elastic modulus of 60 GPa and a Poisson's ratio of 0.2. Contact elements were inserted at the interfaces between neighboring plies of the same layer to prevent interpenetration. The EVA interlayer was modeled with nonlinear cohesive elements and a mode-II triangular cohesive law (Fig. 9b). The maximum traction of the cohesive law was set to 3.2 MPa, which was obtained from the lap shear tests on the EVA interlayer on glass substrates. We used a maximum displacement jump of 10 mm and tuned the initial slope of the cohesive law in order to match the tensile response of the $\theta = \pm 75^\circ$, which failed by translational mode of the plies (the $\theta = \pm 75^\circ$ sample was the closest from a shear lap experiment). For all models the mesh was refined to ensure convergence in terms of the force-displacement curves as well as local stresses. Fig. 9c shows that the finite element models could successfully capture the experimental trends, but that they overestimated in general the strength of material. We attributed this discrepancy to defects in the physical samples which can decrease their overall properties, and to the simplified failure criteria we used in the finite element models. Stiffness and strength both increase when the ply width is increased, or when the ply angle is decreased because higher d and/or lower θ result in an increase of overlap area. In some experiments individual plies fractured, which interrupted the mechanisms of ply rotation and/or sliding

and precipitated brittle fracture. The finite element models revealed that the highest stresses in the plies are due to flexion, with maximum stress values at the edges of the plies (Fig. 9d). To predict the onset of ply fracture we simply compared the maximum principal stresses in the plies with the tensile strength for laser cut borosilicate glasses (70 MPa measured by bending tests no shown here). The predictions in terms of ply fracture and brittle are consistent with the experiments: In samples with lower ply angles ply fracture is the dominant failure mode, which leads to an overall brittle type of failure for the materials. In contrast, the model predicts that the plies of the samples with high ply angle remain intact, which is consistent with the experiments.

The model also captures the main trends and deformation modes observed experimentally in the post yield regions. The $\theta = \pm 75^\circ$ cross-ply primarily fail by the translational mode, and the $\theta = \pm 45^\circ$ and $\theta = \pm 60^\circ$ architectures deform and fail by the rotational and brittle ply fracture modes, respectively (Fig. 9e). Fig. 9f shows that the rotation of plies is prominent for smaller ply angles. At lower ply angles, although the plies can rotate with deformation, the plies carry high bending stresses that make the plies fracture prematurely (Fig. 9e).

A striking feature of the architected glass is its ability to delay strain localization and distribute deformation over large volumes even in the post-yielding stage. We explored this mechanism in depth using our finite element models. Even though the cohesive law softens in the post yield region (Fig. 9b), the architected glass can display constant post-yield tensile stress ($\theta = \pm 60^\circ$) or even strain hardening (case $\theta = \pm 45^\circ$, Fig. 9c), with the direct effect of delaying strain localization. To explain this phenomenon, we focus on the distribution of shear stress at the interlayer (Fig. 9f). Cases $\theta = \pm 60^\circ$ and $\theta = \pm 45^\circ$ show a non-uniform distribution of

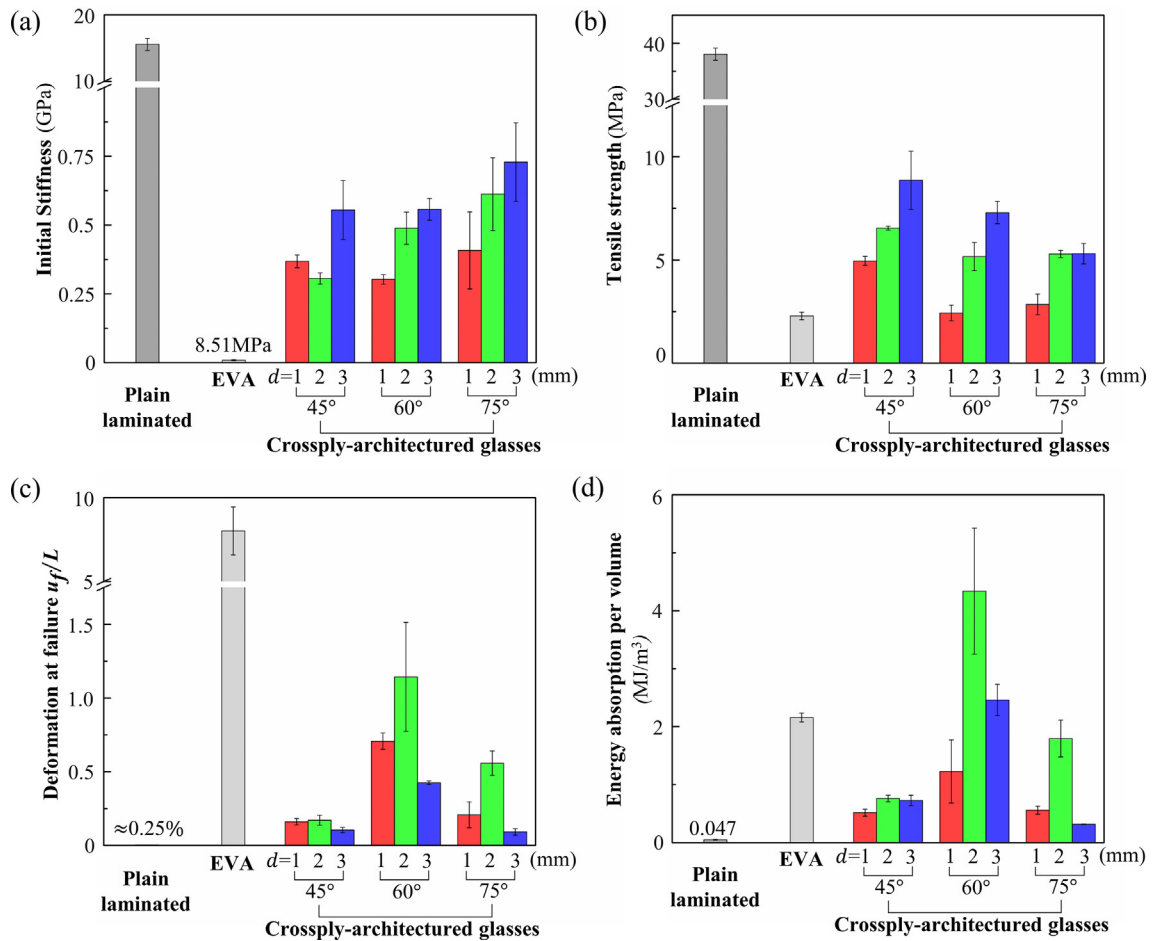


Fig. 8. Tensile properties for plain laminated glass, pure EVA and architected cross-ply glasses: (a) Initial stiffness; (b) tensile strength; (c) deformation at failure and (d) energy absorption based on the failure criterion that the nominal stress drops below the yielding strength of EVA.

shear stresses that results from the rotation of the plies superimposed to the uniform shear stress from ply separation. The profiles display regions where the shear stress is positive, and regions where it is negative. The center of rotation (where $\tau_{xz} = 0$ and $\tau_{yz} = 0$) is slightly off-centered, so that the distribution produces a net tensile force within the material. Fig. 10 shows the evolution of the shear distribution for the case $d = 2$ mm, $\theta = \pm 45^\circ$. Both series of snapshots were taken in the post-yield region, at $u/L = 0.08$ and $u/L = 0.48$. The region of interest can be conveniently divided into four sectors. Fig. 10 shows the net force vector transmitted by the interlayer through each of the sectors, computed from the distribution of shear stresses τ_{xz} and τ_{yz} . Three concurrent effects are visible as the global deformation is increased: (i) The magnitudes of the traction forces exerted on each of the four sectors decrease; (ii) the center of rotation shifts towards the left, so that the region that produces tensile traction forces increases in size; (iii) the traction force vectors rotate and align towards the pulling direction. The first effect is due to the inherent softening of the cohesive law, contributing to global softening. This effect is however offset by the second and third effects. As the region producing negative (blue) traction decreases, the net force increases. As all traction vectors align toward the direction of pulling, their projection along that direction increase, which produces an increasing global force even though the magnitude of each of the four traction vector decreases. These results demonstrate how architecture and large rotational kinematics can produce strain hardening from strain softening materials. This unique mechanism provides the cross-ply glasses with a nearly 100 times amplification of deformability

and energy absorption compared to plain laminated glass. The case $\theta = \pm 75^\circ$ does not produce any ply rotation so that these effects are completely absent. As a result, this case produces materials which soften with deformation and when localize deformation prematurely.

6. Notch performance and toughness

We finally assessed the fracture toughness and notch performance of our architected cross-ply glasses. These properties can be interpreted as their tensile performance in the presence of a severe stress concentration, which is critical for robustness and damage tolerance. Mode-I fracture tests were performed on compact tension samples on both the plain laminated samples and the cross-ply samples, with geometry and dimensions shown on Fig. 11a. The overall geometry of the sample (including in-plane dimensions, notch depth and thickness) was kept identical across all samples. The notch was cut using the 355 nm UV laser at a power of 400 mw with a defect spacing of 5 μm . Since the defects generated by the laser consist of microcracks [21], the tip of the initial notch was perfectly sharp. Both plain laminated glass (Fig. 11b) and cross-ply architected glass (Fig. 11c) were tested using the same loading stage as for the tensile tests, at a rate of 5 $\mu\text{m/s}$.

Fig. 11d shows typical force-displacements for regular and architected glasses. As expected, plain laminated glass performed poorly in the presence of a notch, with a greatly reduced

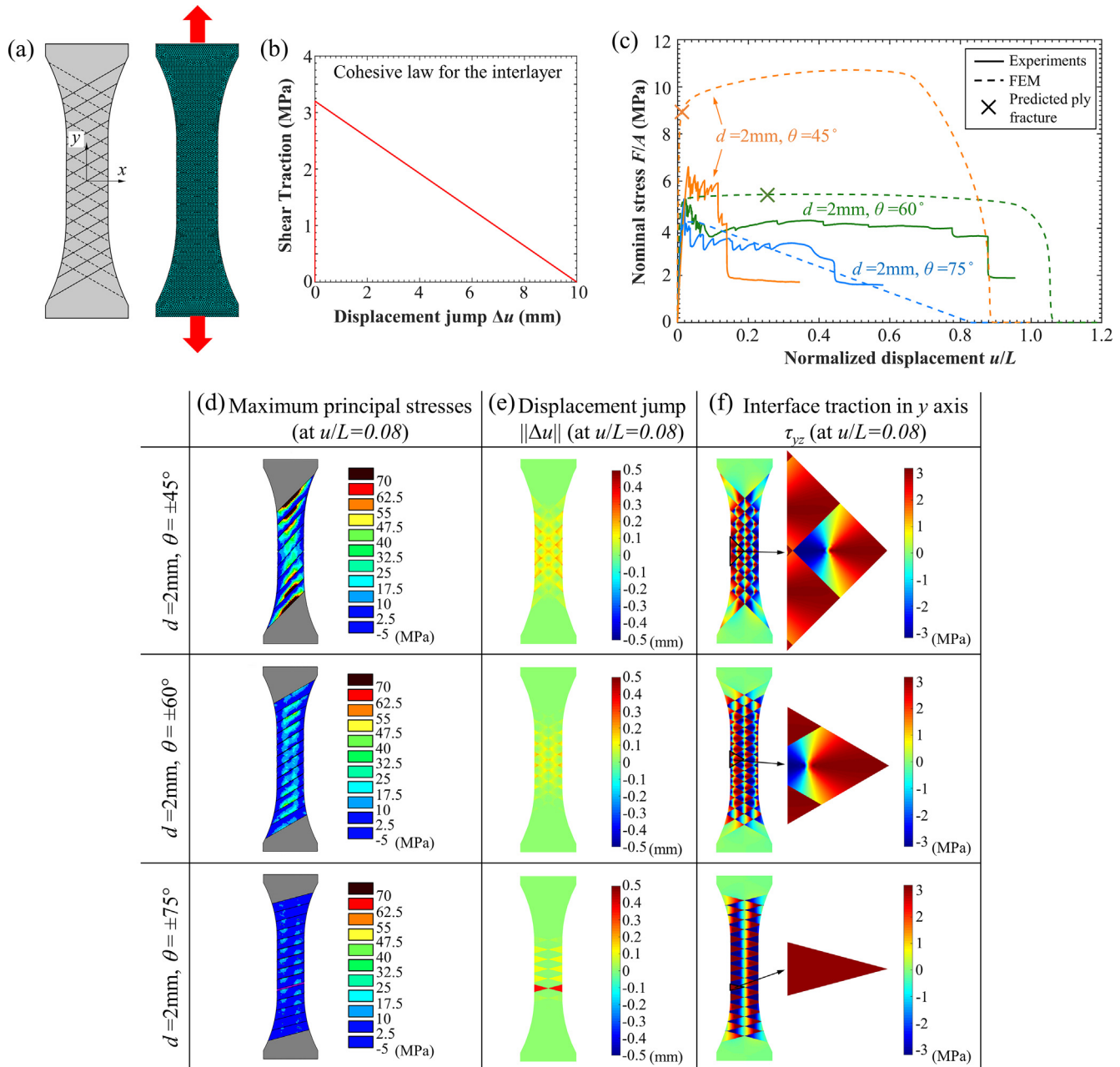


Fig. 9. (a) Finite element model setup; (b) Cohesive law simulating the shear response of the EVA interlayer; (c) Experimental and finite elements force-displacement; (d) Maximum first principal stresses in the plies; (e) Displacement jump Δu across the layers and (f) distribution of shear tractions at the interlayer.

tensile strength. Crack propagation was rapid and straight, and the overall response was brittle. In contrast, the crack path in the architected glass was convoluted, with multiple deflections and crack twisting and large energy to fracture. Crack propagation was stable, and the force-displacement curve had a general bell curve with multiple drops in the softening region. The peak force F_{max} marked the point where crack propagation commenced, although some inelastic activity was usually observed on the loading part of the curve. The force required to initiate cracking F_{max} in the architected glass was 1.4 to 4 times higher than in plain laminated glass ($p < 0.05$, Fig. 12a). This result demonstrates that powerful toughening mechanisms such as crack blunting of the crack, twisting of the crack front, mixed mode and inelastic deformations ahead of the crack operate to resist the onset of crack propagation. We also compared the nominal strength of the materials with and

without the presence of a notch, in order to determine their tolerance to stress concentration. Fig. 12b shows the ratio between the nominal strength from a notched sample to the tensile strength from an un-notched tensile test. The ratio for traditional laminated glass is less than 0.05 which is expected, these materials do not tolerate damage well and damaged laminated windows or windshields must be replaced as soon as a small amount of damage is detected. The cross-ply architected glasses performed much better, with a strength ratio ranging from 0.4 to 1. This result clearly demonstrates how the micromechanics associated with the cross-ply architecture can mitigate or even entirely suppress the effects of stress concentrations from sharp geometrical features, defects or cracks. Extremely tough materials can even become notch insensitive, which mean that they completely suppress stress concentrations by way of inelastic deformations (Fig. 12c).

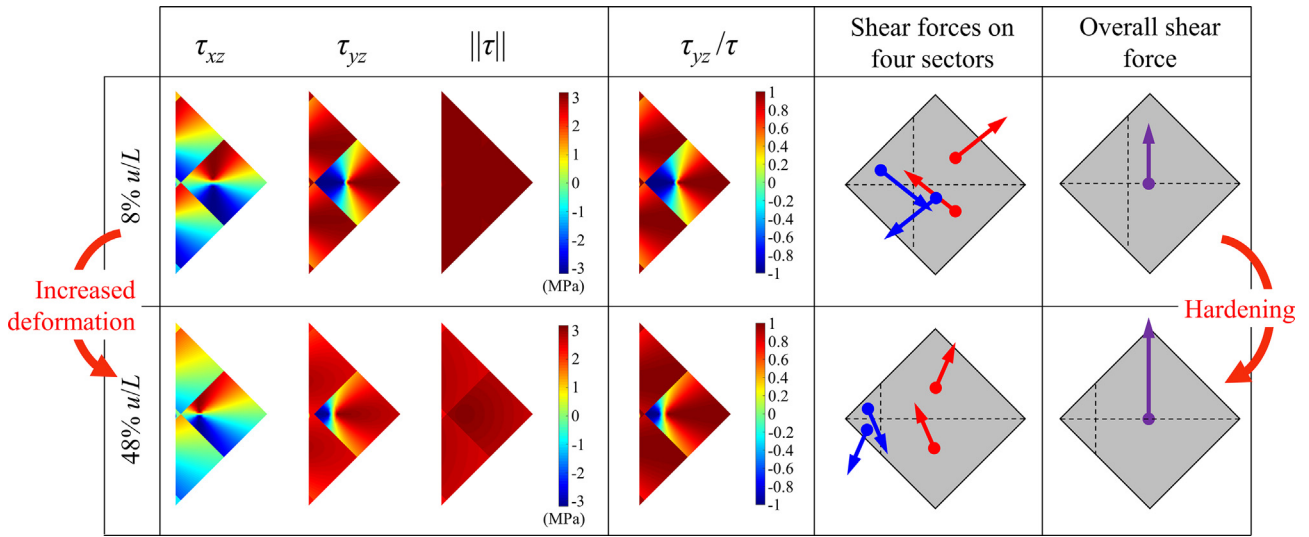


Fig. 10. Local shear stresses τ_{xz} , τ_{yz} , magnitude of shear stress τ , distribution of τ_{yz}/τ , schematic showing the change of magnitude and direction of force vectors on four different sectors at the interlayer and resulting overall force. Each data is given at two level of deformation in post yield regime. These results demonstrate how global strain hardening can be attained from a softening interface.

We finally measured the resistance to fracture of the material, by estimating the energy required to completely fracture the samples. Since the ductile interlayer maintained a nonzero force even after the glass architecture has collapsed, for the purpose of computing U we assumed that the sample had failed when the force had decreased to $0.45F_{max}$ (Fig. 12d). To compare the different materials in terms of notch tolerance and toughness, we used a nominal strength defined as: $F_{max}/(b - a)t$ and the work of fracture defined as $U/(b - a)t$ where $(b - a)t$ is the cross sectional area of the ligament (Fig. 11a). Fig. 12b shows the work of fracture for the configurations tested here. The work of fracture of traditional laminated glass obtained from the force-displacement curves is very small (~ 0.04 kJ/m²), because once the crack propagates there is no significant toughening mechanisms in that material. In our cross-ply architected glasses the work of fracture was 12 to 53 times higher than that of the plain laminated glasses. In addition, because crack propagation in traditional laminated glass is sudden and brittle, a large portion of the energy accumulated prior to fracture may be dispelled in dynamic effects instead of by creating new fracture surfaces. For brittle materials, the real work of fracture may represent as little as half of the strain energy stored in the sample at the onset of fracture [32]. With this correction for dynamic energy considered, the work of fracture of our

architected glass may have been up to 100 times higher than plain laminated glass. Within the results for architected glass we did not observe a simple trend of the work of fracture with ply angle θ and ply width d , which we attributed this effect to different failure modes we observed across these designs. Fig. 12e shows the three fracture modes we identified for the cross-ply architected glasses, as function of ply angle and ply width. The snapshots of that figure and in-situ observations showed that in general, when the crack reaches an interface between the plies, it is either deflected by the interface or it penetrates through the plies. When the crack was deflected its path was different in each layer, which triggered additional toughening mechanisms such as crack bridging by the plies and plastic deformation of the interlayer, improving energy absorption and impeding crack propagation. In general, fracture of individual plies was therefore detrimental to overall toughness. The first mode is the crack deflection mode, which was prominent for low ply angle. In this mode the cracks were deflected along the weak interface, which stabilized crack propagation and increased toughness in a way similar to multilayered ceramics [33]. Fracture of individual plies was however also prominent in that mode. In this particular mode we found that the work of fracture was higher for smaller ply width d , because there were more weak interfaces to deflect the

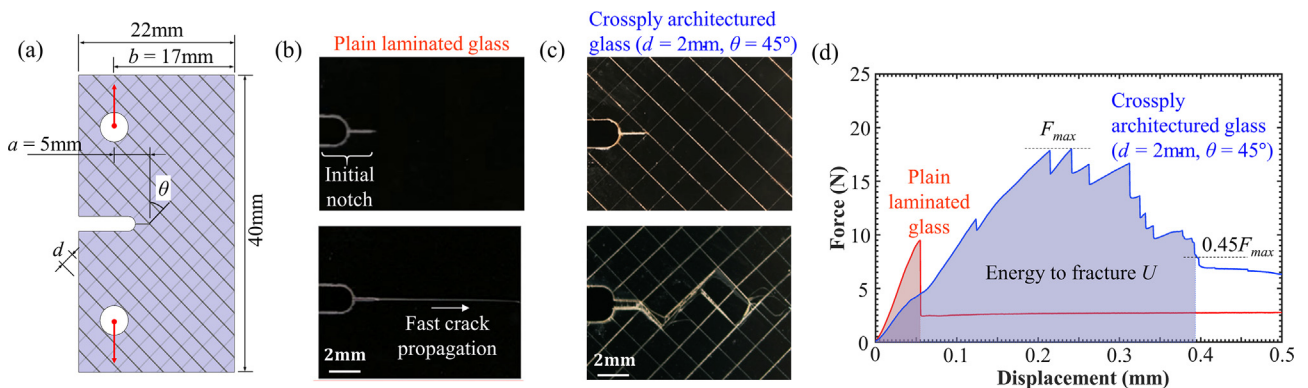


Fig. 11. (a) Dimensions of fracture test samples; (b) Straight and rapid crack propagation in plain laminated glass; (c) progressive and twisted crack propagation in cross-ply architected glass; (d) typical tensile notched force-displacement curves for plain laminated glass and for cross-ply architected glass.

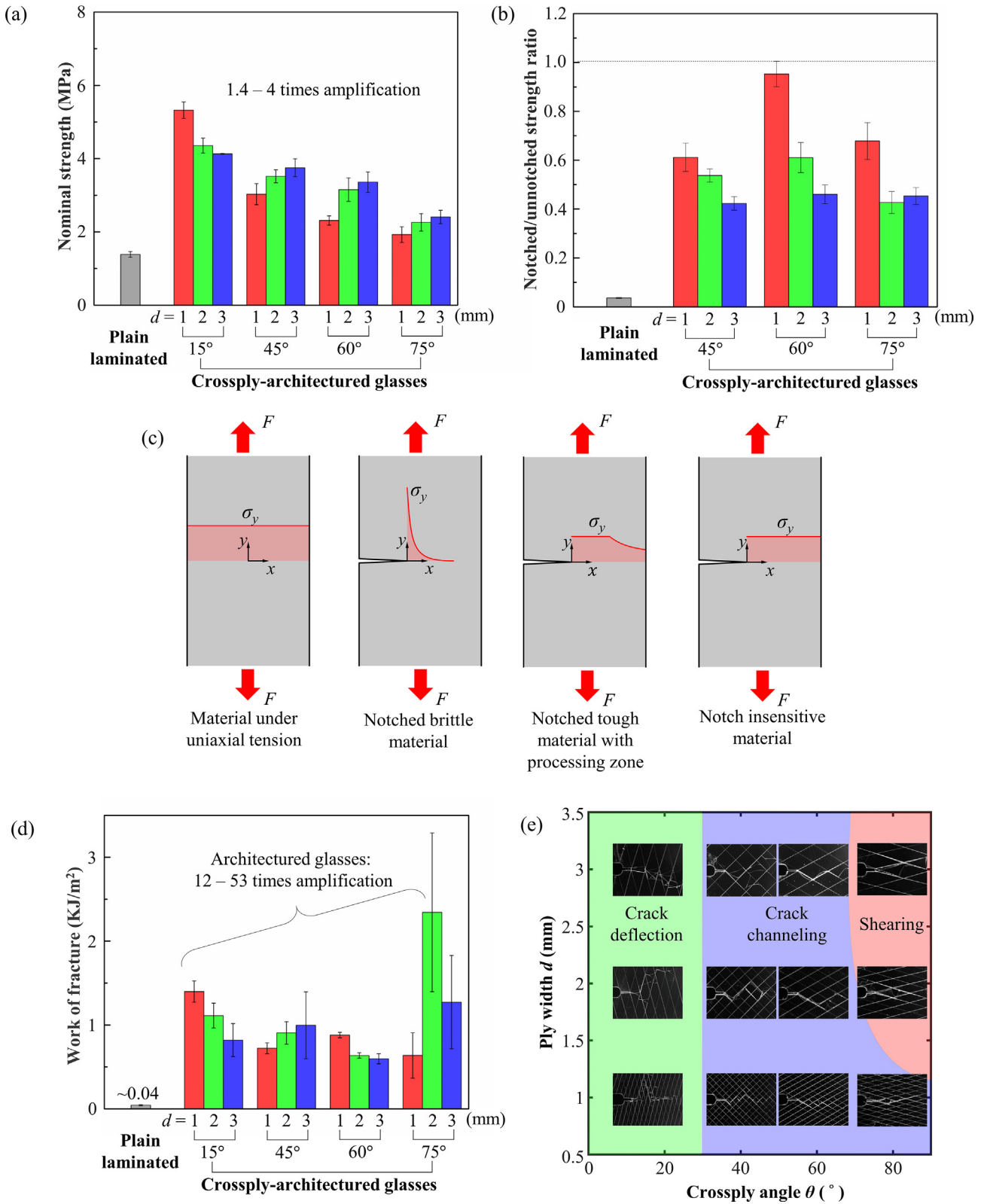


Fig. 12. (a) Nominal strength of the notched samples for different configurations; (b) Ratio of notched and unnotched strength (a ratio of 1 means that the material is notch insensitive); (c) Illustration showing how tough and deformable materials redistribute stresses at a notch; (d) Work of fracture for different laminated glass designs; (e) Failure mode map as function of ply angle θ and ply width d .

crack. At intermediate ply angles, crack channeling mode prevailed, where crack deflection was accompanied by shearing of the interfaces. The dominant toughening mechanism in this mode is the crack bridging by the plies, and the effect of ply width on work of fracture was minimal.

The third fracture mode was the shearing mode which we observed for the highest ply angle ($\theta = 75^\circ$). In this fracture mode crack deflection was prominent, with a crack path which was different in the two layers so that fracture resistance was mostly generated by the shear deformation of the interlayer. In the third fracture mode, the intermediate ply width $d = 2$ mm achieved the highest work of fracture ($p < 0.05$). For a lower ply width $d = 1$ mm, the overlap area was too small to provide enough resistance and energy absorption. For a higher ply width ($d = 3$ mm), the overlap areas were too large which caused the premature failure of individual glass plies. The optimal failure mode depends on the working environment and the potential applications of the material. The shearing mode has a more progressive crack propagation and the most work of fracture but it produces a relatively low nominal strength in general. The crack deflection mode has the highest nominal strength but its work of fracture is not always the most optimal. In most of cases, the crack deflection mode should probably be promoted due to its stable performances and the balance between nominal strength and work of fracture.

7. Conclusions

Conch shells, fish scales or arthropod shells [14–16] demonstrate how the cross-ply architecture generates powerful toughening mechanisms that include crack deflection, twisting and crack bridging [17]. The toughest of these materials also rely on large deformations at the interfaces between plies or fibers, which generates large strains, energy dissipation and fiber rotation towards the axis of pulling [15,34]. Here we duplicate biological cross-ply architectures and their associated mechanisms in a new laminated glass designs that generate new combination of toughness, deformability, and damage tolerance. The main conclusions are as follows:

- (i) The laser engraving approach we use generates cross-ply and interfaces in laminated glass that can guide and channel cracks and deformation, with little impact on surface hardness and optical quality. The crossply architecture can be finely tuned to change the micromechanics of deformation, the overall performance and the mechanisms of fracture.
- (ii) Remarkably, we show that strain hardening and delocalization of strains can be achieved from large rotation of the plies, even if a softening interlayer is used. Our results also emphasize the idea that weak but deformable adhesive are preferable as interlayer over stronger but more brittle adhesives.
- (iii) Overall our best cross-ply design has a strength which is 4 times lower than laminated glass in uniaxial tension of intact samples, but it can absorb up 100 times more energy by controlled inelastic deformation of the interlayer. In the presence of a severe stress concentration, our materials perform much better than traditional laminated glasses, demonstrating a high capability for damage tolerance. These results demonstrate how the interplay between hard materials with controlled architected and soft interlayers can produce outstanding properties.
- (iv) The nature of architected materials creates theoretical difficulties with implications in the laboratory: (1) the size of the architecture approaches the size of the entire sample, so that separation of length scales is not possible and (2) for most architected samples the size of the inelastic

region also approached the size of the sample. For these reasons the principle of autonomy (a cornerstone of predictive fracture mechanics) was not valid for the samples we tested [35] and we did not attempt to use measures of fracture resistance such as K_{IC} , G_C or J integrals for our materials. In this work we used work of fracture instead, and only to evaluate the resistance to cracking of our architected glasses in comparison with regular laminated glasses tested using the same sample geometry and conditions.

This new type of bioinspired laminated glass has therefore potential in architectural glass, glass curtain walls, electronic device and solar panels. More generally, our material also demonstrates how material architectures at intermediate length scales (mm) can completely change the behavior of material and can generate high performance. In particular, the architecture can be finely tuned to fully exploit the synergies between very hard (but brittle) and very soft (but deformable) components, leading to large amplifications of properties. With this approach superior materials can be synthesized even with inferior base materials, which further expands the design space of the conventional materials. Our future studies on this material include models for fracture so that the exact fracture mode map can be refined, effects of strain rate (including strain rate hardening), and mechanical response under combined loading as done for staggered composites [36].

Acknowledgments

This research was supported by a NSERC Strategic Grant. Z.Y. was partially supported by a McGill Engineering Doctoral Award. The author also thanks Rob Botmann from Glassopolis (Toronto, ON Canada) for valuable discussions and feedback.

References

- [1] K. Burrows, V. Fthenakis, Glass needs for a growing photovoltaics industry, *Sol. Energy Mater. Sol. Cells* 132 (2015) 455–459.
- [2] R.O. Ritchie, The conflicts between strength and toughness, *Nat. Mater.* 10 (11) (2011) 817–822.
- [3] H.S. Norville, W.K. Kim, J. Swofford, Behavior and strength of laminated glass, *J. Eng. Mech.* (1998).
- [4] F. Barthelat, Architected materials in engineering and biology: fabrication, structure, mechanics and performance, *Int. Mater. Rev.* 60 (8) (2015) 413–430.
- [5] U.G. Wegst, H. Bai, E. Saiz, A.P. Tomsia, R.O. Ritchie, Bioinspired structural materials, *Nat. Mater.* 14 (1) (2015) 23–36.
- [6] L.T. Kuhn-Spearing, H. Kessler, E. Chateau, R. Ballarini, A.H. Heuer, Fracture mechanisms of the *Strombus gigas* conch shell: implications for the design of brittle laminates, *J. Mater. Sci.* 31 (1996) 6583–6594.
- [7] R. Menig, M.H. Meyers, M.A. Meyers, K.S. Vecchio, Quasi-static and dynamic mechanical response of *Strombus gigas* (conch) shells, *Mater. Sci. Eng.* 297 (1–2) (2001) 203–211.
- [8] M.A. Meyers, P.-Y. Chen, A.Y.-M. Lin, Y. Seki, Biological materials: Structure and mechanical properties, *Prog. Mater. Sci.* 53 (1) (2008) 1–206.
- [9] S. Kamat, X. Su, R. Ballarini, A.H. Heuer, Structural basis for the fracture toughness of the shell of the conch *Strombus gigas*, *Nat. Mater.* 405 (2000) 1036–1040.
- [10] S. Kamat, H. Kessler, R. Ballarini, M. Nassirou, A.H. Heuer, Fracture mechanisms of the *Strombus gigas* conch shell: II-micromechanics analyses of multiple cracking and large-scale crack bridging, *Acta Mater.* 52 (8) (2004) 2395–2406.
- [11] M. Yahyazadehfar, D. Bajaj, D.D. Arola, Hidden contributions of the enamel rods on the fracture resistance of human teeth, *Acta Biomater.* 9 (1) (2013) 4806–4814.
- [12] F. Barthelat, Z. Yin, M.J. Buehler, Structure and mechanics of interfaces in biological materials, *Nat. Rev. Mater.* 1 (4) (2016) 16007.
- [13] M. Yahyazadehfar, D. Arola, The role of organic proteins on the crack growth resistance of human enamel, *Acta Biomater.* 19 (2015) 33–45.
- [14] D. Zhu, C.F. Ortega, R. Motamedi, L. Szewciw, F. Vernerey, F. Barthelat, Structure and mechanical performance of a “modern” fish scale, *Adv. Eng. Mater.* 14 (4) (2012) B185–B194.
- [15] W. Yang, V.R. Sherman, B. Gludovatz, M. Mackey, E.A. Zimmermann, E.H. Chang, E. Schaible, Z. Qin, M.J. Buehler, R.O. Ritchie, M.A. Meyers, Protective role of *Arapaima gigas* fish scales: structure and mechanical behavior, *Acta Biomater.* 10 (8) (2014) 3599–3614.

- [16] Y. Bouligand, Twisted fibrous arrangements in biological materials and cholesteric mesophases, *Tissue Cell* 4 (2) (1972) 192–217.
- [17] N. Suksangpanya, N.A. Yaraghi, D. Kisailus, P. Zavattieri, Twisting cracks in Bouligand structures, *J. Mech. Behav. Biomed. Mater.* 76 (2017) 38–57.
- [18] G. Karambelas, S. Santhanam, Z.N. Wing, Strombus gigas inspired biomimetic ceramic composites via SHELL—Sequential Hierarchical Engineered Layer Lamination, *Ceram. Int.* 39 (2) (2013) 1315–1325.
- [19] L.K. Grunenfelder, N. Suksangpanya, C. Salinas, G. Milliron, N. Yaraghi, S. Herrera, K. Evans-Lutterodt, S.R. Nutt, P. Zavattieri, D. Kisailus, Bio-inspired impact-resistant composites, *Acta Biomater.* 10 (9) (2014) 3997–4008.
- [20] L. Chen, R. Ballarini, H. Kahn, A.H. Heuer, Bioinspired micro-composite structure, *J. Mater. Res.* 22 (01) (2011) 124–131.
- [21] M. Mirkhalaf, A.K. Dastjerdi, F. Barthelat, Overcoming the brittleness of glass through bio-inspiration and micro-architecture, *Nat. Commun.* 5 (2014) 3166.
- [22] J.C. Weaver, G.W. Milliron, A. Miserez, K. Evans-Lutterodt, S. Herrera, I. Gallana, W.J. Mershon, B. Swanson, P. Zavattieri, E. DiMasi, D. Kisailus, The Stomatopod dactyl club: a formidable damage-tolerant biological hammer, *Science* 336 (2012) 1275–1280.
- [23] ASTM, Standard Test Method for Transparency of Plastic Sheeting, West Conshohocken, PA, 2015.
- [24] H.A. Becerril, J. Mao, Z. Liu, R.M. Stoltenberg, Z. Bao, Y. Chen, Evaluation of solution-processed reduced graphene oxide films as transparent conductors, *ACS Nano* 2 (3) (2008) 463–470.
- [25] B. Pukánszky, Optical clarity of polypropylene products, in: J. Karger-Kocsis (Ed.), *Polypropylene*, Springer, Dordrecht, 1999.
- [26] ASTM, Standard Test Method for Tensile Strength of Monolithic Advanced Ceramics at Ambient Temperatures, West Conshohocken, PA, 2015.
- [27] M. Ostoja-Starzewski, Material spatial randomness: From statistical to representative volume element, *Probab. Eng. Mech.* 21 (2) (2006) 112–132.
- [28] D. Raabe, C. Sachs, P. Romano, The crustacean exoskeleton as an example of a structurally and mechanically graded biological nanocomposite material, *Acta Mater.* 53 (15) (2005) 4281–4292.
- [29] P.Y. Chen, A.Y. Lin, J. McKittrick, M.A. Meyers, Structure and mechanical properties of crab exoskeletons, *Acta Biomater.* 4 (3) (2008) 587–596.
- [30] F. Barthelat, A.K. Dastjerdi, R. Rabiei, An improved failure criterion for biological and engineered staggered composites, *J. R. Soc Interface* 10 (79) (2013) 20120849.
- [31] ANSYS, ANSYS® Academic Research, 2015.
- [32] S.M. Barinov, Work-of-fracture determination for brittle materials, *J. Mater. Sci. Lett.* 12 (1993) 674–676.
- [33] W.J. Clegg, K. Kendall, N.M. Alford, T.W. Button, J.D. Birchall, A simple way to make tough ceramics, *Nature* 347 (1990) 455–457.
- [34] A. Khayer Dastjerdi, F. Barthelat, Teleost fish scales amongst the toughest collagenous materials, *J. Mech. Behav. Biomed. Mater.* 52 (2015) 95–107.
- [35] A.T. Zehnder, *Fracture Mechanics*, Springer, Netherlands, 2012.
- [36] V. Slesarenko, N. Kazarinov, S. Rudykh, Distinct failure modes in bio-inspired 3D-printed staggered composites under non-aligned loadings, *Smart Mater. Struct.* 26 (3) (2017) 035053.